GEOPHYSICAL RESEARCH LETTERS, VOL. 35, L23203, doi:10.1029/2008GL035947, 2008

Shocked H_2O ice: Thermal emission measurements and the criteria for phase changes during impact events

Sarah T. Stewart,[1] Achim Seifter,[2] and Andrew W. Obst[2]

Received 9 August 2008; revised 28 October 2008; accepted 30 October 2008; published 6 December 2008.

[1] Impact cratering events on icy planetary bodies may produce transient liquid water and vapor. We present the first thermal emission measurements from shocked H_2O ice and derive peak and post-shock temperatures. Under shock pressures between 8.2 and 13.6 GPa, initially ~165 K ice is heated to between 673 and 1055 K. In the time frame of the experiment, the shocked H_2O releases to the saturation vapor curve and does not achieve full decompression. The temperature results are used to validate the new 5-Phase H_2O model equation of state (EOS). The 5-Phase EOS is used to predict the critical shock pressures required to induce melting and vaporization of ice for a wide range of ambient pressures and temperatures. Impact events with velocities as low as ~1 km/s will initiate phase changes on icy surfaces. Thus, shock-induced melting and vaporization of ice is a widespread process in the solar system. **Citation:** Stewart, S. T., A. Seifter, and A. W. Obst (2008), Shocked H_2O ice: Thermal emission measurements and the criteria for phase changes during impact events, *Geophys. Res. Lett.*, *35*, L23203, doi:10.1029/2008GL035947.

1. Introduction

[2] Impact cratering is one of the major geologic processes in the solar system. Impact-induced phase changes are a particularly important process in the evolution of the surfaces of icy planets and satellites. For example, melting and vaporization of ice during impact events may redistribute volatile reservoirs and create transient, water-rich habitats. Numerical simulations of impact events have been used to infer the production and amounts of transient liquid water on Mars and Titan [*Artemieva and Lunine*, 2003; *Stewart et al.*, 2004; *Artemieva and Lunine*, 2005; *Pierazzo et al.*, 2005] and to estimate the thickness of the brittle ice crust on Europa [*Turtle and Pierazzo*, 2001]. In addition, the post-shock temperature field is important for rheological models of H_2O ice, which in turn affects the observed crater morphologies [e.g., *Senft and Stewart*, 2008]. These computational studies rely on a model equation of state for H_2O to infer the post-impact temperature field and the occurrence of phase changes.

[3] Here, we present peak and post-shock temperature measurements from shock pyrometry experiments on H_2O ice. The results are used to validate the temperature and entropy in the new 5-Phase H_2O model EOS [*Senft and Stewart*, 2008] and to derive the criteria for shock-induced phase transformations during impact events on icy planetary bodies.

2. Experimental Method and Data Analysis

[4] Specimens of transparent, polycrystalline, columnar ice were grown from degassed, distilled water. The typical column width was 3 to 4 mm. Target ice samples were cored in the columnar direction and cut into nominally 31 × 3 mm discs.

[5] Planar shock waves, with peak pressures between 8 and 14 GPa, were generated in ice using the Harvard 40-mm single stage powder gun. Ice samples were mounted on an aluminum driver plate and enclosed in an 1×10^{-4} Pa (~1 microtorr) vacuum chamber with a downrange CaF_2 window for optical and infrared measurements. The driver plate was cooled by liquid nitrogen. Simultaneous particle velocity and radiance measurements were recorded from the downrange face of the sample. The experimental configuration is described in previous work [*Seifter et al.*, 2006; *Stewart et al.*, 2006] and in the auxiliary materials[1]. The ice sample temperature was maintained at ~150 K (sufficiently cold to prevent significant sublimation under vacuum), and at the time of the experiment the ice temperatures were 165 ± 11 K.

[6] Time-resolved emission was collected by a photomultiplier tube filtered at 0.65 μm and a near-infrared (NIR), four-band (centered at 1.8, 2.3, 3.5, 4.8 μm) pyrometer built at Los Alamos National Laboratory [*Boboridis et al.*, 2003]. The NIR pyrometer is sensitive to radiance temperatures as low as room temperature and has a temporal resolution of ~17 ns. Free surface particle velocities were recorded by a Velocity Interferometer System for Any Reflector (VISAR) [*Barker and Hollenbach*, 1972]. The VISAR data provides a reference for the time of shock release in the thermal emission measurements.

[7] The peak shock pressure was derived from the impedance match solution using the measured impact velocity and known Hugoniots for the flyer, driver, and ice sample (Table S1). The compression and peak temperature is expected to be homogeneous because the peak shock pressures are much greater than the Hugoniot Elastic Limit (~0.5 GPa [*Stewart and Ahrens*, 2005]).

[8] Typical NIR radiance data are shown in Figure 1. When the shock reaches the driver-ice interface, we observe a radiance spike, which probably arises from trapped air and/or surface roughness as no adhesive material was used. At 1.8 and 2.3 μm, the observed emission then rises due to the decrease in absorption length as the shock wave travels through the sample. At 3.5 and 4.8 μm, ice is too absorbing

[1]Department of Earth and Planetary Sciences, Harvard University, Cambridge, Massachusetts, USA.
[2]Los Alamos National Laboratory, Los Alamos, New Mexico, USA.

0094-8276/08/2008GL035947$05.00

[1]Auxiliary materials are available in the HTML. doi:10.1029/2008GL035947.

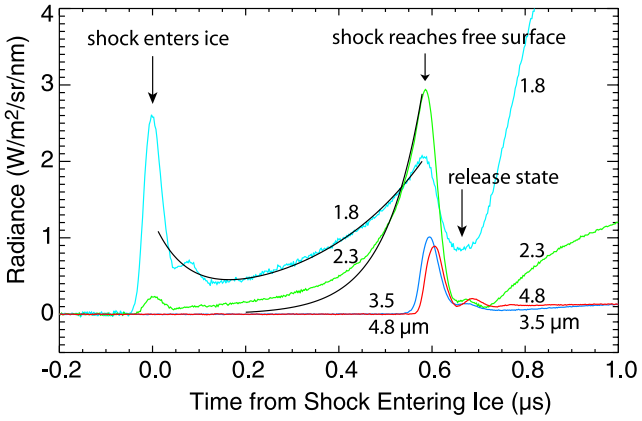

Figure 1. Near-infrared thermal emission data record from H_2O ice shocked to 13.6 GPa. Black lines are fits using equation (1).

to observe the propagating shock wave. Upon shock release by wave reflection at the downrange free surface, the radiance drops. At later times, the arrival of non-planar waves changes the observed radiance.

[9] We derived the peak shock temperatures following the method of *Luo et al.* [2004]. The observed radiance (L_{obs}) at 1.8 and 2.3 μm were fit by

$$L_{obs} = L_{driver} e^{-a_s d_s} e^{-a_u d_u} + L_{H_2O}\left(1 - e^{-a_s d_s}\right) e^{-a_u d_u}, \qquad (1)$$

where L_{driver} is the radiance from the driver-ice interface (attenuated by the shocked and unshocked ice) and L_{H_2O} is the radiance from the shock front (attenuated by the unshocked ice). L_{driver}, L_{H_2O} and the absorption coefficients (a_u for unshocked and a_s for shocked H_2O) are fitted as a function of time using the changing thickness of H_2O on either side of the shock front (d_u for unshocked and d_s for shocked) (see auxiliary materials for fits). The fitted absorption coefficients for unshocked ice are in excellent agreement with measured values [*Hale and Querry*, 1973]. Note that the driver interface contribution likely includes a time decaying component that was masked by the high absorption of shocked H_2O. Radiance is converted to temperature using the Planck function. Reported peak shock temperature values are averages of the 1.8 and 2.3 μm fits.

[10] The temperatures of the shock released state are calculated using the average of the 3.5 and 4.8 μm channels, during the plateau after the shock reaches the free surface and using an emissivity of 1 (in agreement with the high absorption coefficients at these wavelengths). The 1.8 and 2.3 μm data are not used to derive post-shock temperature as the emission is dominated by the peak shock signal through the transparent sample.

3. Shock Temperature Results

[11] In experiments reaching shock pressures between 8.2 and 13.6 GPa, initially ~165 K ice is compressed and heated to between 673 and 1055 K (Figure 2, solid symbols). The observed temperatures after shock release fall between 382 and 530 K (Figure 2, open symbols). Data are compiled in Table S2.

[12] In Figure 2, we compare the temperature data to the Hugoniot and shock release isentropes from the 5-Phase H_2O model EOS [*Senft and Stewart*, 2008]. The 5-Phase EOS includes three solid phases (ices Ih, VI, and VII), liquid, and vapor. The EOS of the phases and phase boundaries are based on fits to experimental data. The development of the 5-Phase EOS is described in detail by *Senft and Stewart* [2008]. Although the model peak shock temperatures are about 10% lower (or about 1 to 2 standard deviations) than observed at a given shock pressure, the 5-Phase EOS is a very significant improvement over previous, commonly used EOS models for H_2O (Figure S6). The magnitude of the mismatch cannot be accounted for by the uncertainty in the initial temperature. The observed post-shock temperatures are much higher than expected for full release to the ambient pressure in the sample capsule. Based on previous thermodynamic calculations and pressure-volume Hugoniot measurements [*Stewart and Ahrens*, 2005], we expected release temperatures on the sublimation curve, at about 160 K (below our measurement limits).

[13] The release temperature data are explained by examination of the H_2O temperature-entropy phase diagram (Figure 3). The temperature data are plotted using the model entropy on the 5-Phase EOS 165-K Hugoniot (grey line) for the peak shock pressure of each experiment. The data are compared to experimental phase boundaries (black lines) [*Wagner and Pruss*, 2002]. In the lowest pressure experiment (circle), the peak shock state lies in (or near) the ice VII-liquid mixed phase region; in the rest of the experiments, the peak shock state is a supercritical fluid. Unloading from the shock state is isentropic, so the release path is a vertical line.

[14] In Figure 3, the released states clearly lie on the saturation vapor curve. In these experiments, the shocked H_2O initially unloads to the liquid-vapor phase boundary, and continued decompression requires transformation to a mixture of liquid and vapor. Hence, complete decompression requires a significant volume expansion, and the volume expansion is incomplete during the period of observation.

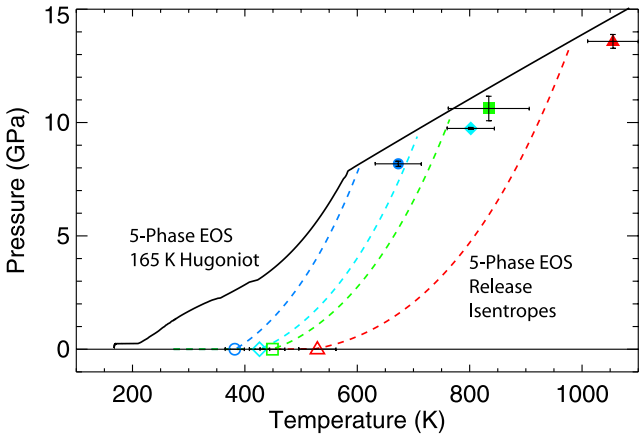

Figure 2. Ice peak (filled symbols) and post-shock (open symbols) temperature data compared to predicted values from the 5-Phase H_2O EOS model (solid and dashed lines). Release isentropes begin on the Hugoniot at the peak pressure for each experiment.

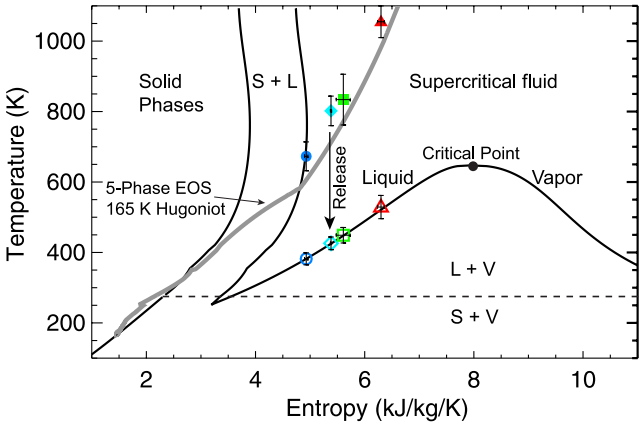

Figure 3. Simplified temperature-entropy phase diagram for H_2O (black lines) with shock and post-shock temperature measurements (closed and open symbols). Dashed horizontal line indicates the triple point temperature; the minimum in the solid-liquid phase boundary (that dips below 273 K) is due to the negatively sloped melting curve for ice Ih.

[15] Based on the observed release temperatures and the known saturation vapor curve, the partially released H_2O is under pressures between 0.14 and 3.85 MPa. Full release to equilibrium at the initial ambient pressure (microtorr or 10^{-4} Pa) would result in temperatures of ~160 K.

[16] We note that the 0.65-μm channel consistently recorded temperatures of ~1900 K during and after shock passage. Although no bubbles are observed in the ice samples under microscopic examination, a plausible explanation of the visible data is trace amounts of trapped air. To determine the possible contribution from air to the observed peak temperatures in the 1.8 and 2.3 μm channels, we fit a two-component mixture of air and H_2O to the visible and NIR data (see method of *Stewart et al.* [2006]). We found that any contribution from air to the observed peak shock temperatures is within the reported errors.

4. Criteria for Shock-Induced Phase Changes

[17] The onset of impact-induced phase changes is dependent on the ambient pressures and temperatures on a particular planetary body. Here, we use the entropy method of *Ahrens and O'Keefe* [1972] to determine the shock pressures required to drive phase transformations in H_2O ice. The entropy of the shocked state is compared to the entropy values required for melting and vaporization as a function of the ambient pressure. In this manner, we derive the critical shock pressure that leads to a phase change upon full release from the shocked state for a wide range of ambient pressures and initial temperatures.

[18] In the regime where shock leads to partial vaporization, the new temperature data on H_2O ice validate the entropies in the 5-Phase EOS. As shown in Figure 3, the entropies on the model Hugoniot are within 2% of the entropies on the experimental saturation vapor curve at the observed release temperatures. Under conditions that lead to complete vaporization, the 5-Phase EOS is validated by comparison to published peak shock temperature measurements on liquid water [*Kormer*, 1968; *Lyzenga et al.*, 1982]. The model temperatures on the liquid water Hugoniot are within 2 to 10% of the measured shock temperatures (2000 to 5300 K) at shock pressures between 30 and 80 GPa (Figure S7). Previous work determined that the criteria for melting is controlled by the formation of high-density polymorphs of ice (ices VI and VII) [*Stewart and Ahrens*, 2005], which are included in the 5-Phase EOS.

[19] Using the entropy values along experimentally determined phase boundaries [*Wagner and Pruss*, 2002] and the 5-Phase EOS, we calculate the critical shock pressure required to induce melting or vaporization upon release to a wide range of ambient pressures (Tables S4 and S5). The entropy in the shock state depends on the initial temperature, and the results for 100 K and 263 K ice are shown in Figure 4. The shock pressures required for phase changes are lower than previous work [*Kieffer and Simonds*, 1980; *Ahrens and O'Keefe*, 1985; *Pierazzo et al.*, 1997] and in good agreement with recent calculations accounting for low-pressure phase changes on the Hugoniot [*Stewart and Ahrens*, 2005].

5. Discussion and Conclusions

[20] Impact velocity is a convenient parameter to determine the onset of shock-induced phase changes during impact events. Figure 4 provides the critical velocities for ice projectiles and ice surfaces. For comparison, the average present-day impact velocities for comets onto the icy moons of the giant planets range from about 3 to 60 km/s [*Zahnle et al.*, 2003]. Mutual collisions between objects in the Kuiper Belt, including Pluto (atmosphere 0.1's Pa), are about 1 km/s [*Trujillo et al.*, 2001]. On Mars (atmosphere ~600 Pa), asteroid impactors have velocities of ~10 km/s [*Ivanov*, 2001]. For the velocities during the late stages of planet formation, collisional growth of icy bodies will be accompanied by shock-induced phase changes that could lead to partial devolatilization [*Ahrens and O'Keefe*, 1985].

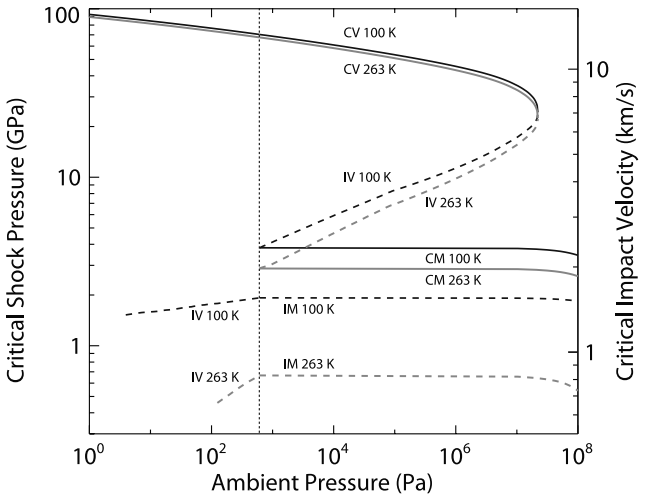

Figure 4. Critical shock pressures and impact velocities (for ice on ice) for incipient and complete melting (IM, CM) and incipient and complete vaporization (IV, CV) of ice initially at 100 K or 263 K versus ambient pressure. Vertical line denotes the triple point pressure.

Hence, with the low impact velocities required for the initiation of melting and vaporization, almost all impact events onto icy bodies will initiate a phase change in ice.

[21] The shock temperature data on ice also highlight the importance of local conditions during impact events on icy bodies. The time scale and thermodynamic path from the shocked to the fully released state will depend upon the ambient pressure and confinement conditions. For example, during crater formation, a parcel of H_2O shocked to a state that will lead to partial vaporization may transiently remain in a superheated liquid state if buried and pressurized. Future work will investigate the behavior of ice shocked into the supercritical state during crater formation and the effect on observed crater forms (e.g., central pit craters [see *Wood et al.*, 1978]). The behavior of shocked H_2O during decompression should lead to a variety of features that depend on the ambient conditions specific to each icy planetary body.

[22] **Acknowledgments.** This work was supported by NASA grant NNX06AC13G and the Harvard Center for Nanoscale Systems (NSF award ECS-0335765). We appreciate the comments from the reviewers and laboratory assistance from Lee Farina and Andrea Peterson.

References

Ahrens, T. J., and J. D. O'Keefe (1972), Shock melting and vaporization of lunar rocks and minerals, *Moon*, *4*, 214–249, doi:10.1007/BF00562927.

Ahrens, T. J., and J. D. O'Keefe (1985), Shock vaporization and the accretion of the icy satellites of Jupiter and Saturn, in *Ices in the Solar System*, *NATO ASI Ser.*, *Ser. C*, vol. 156, edited by J. Klinger et al., pp. 631–654, Kluwer Acad., Boston, Mass.

Artemieva, N., and J. Lunine (2003), Cratering on Titan: Impact melt, ejecta, and the fate of surface organics, *Icarus*, *164*, 471–480, doi:10.1016/S0019-1035(03)00148-9.

Artemieva, N., and J. I. Lunine (2005), Impact cratering on Titan. II. Global melt, escaping ejecta, and aqueous alteration of surface organics, *Icarus*, *175*, 522–533, doi:10.1016/j.icarus.2004.12.005.

Barker, L. M., and R. E. Hollenbach (1972), Laser interferometer for measuring high velocities of any reflecting surface, *J. Appl. Phys.*, *43*, 4669–4675, doi:10.1063/1.1660986.

Boboridis, K., A. Seifter, and A. W. Obst (2003), High-Speed infrared pyrometry for surface temperature measurements on shocked solids, *VDI Ber.*, *1784*, 119–126.

Hale, G. M., and M. R. Querry (1973), Optical constants of water in the 200 nm to 200 micron wavelength region, *Appl. Opt.*, *12*, 555–563.

Ivanov, B. A. (2001), Mars/Moon cratering rate ratio estimates, *Space Sci. Rev.*, *96*(1–4), 87–104, doi:10.1023/A:1011941121102.

Kieffer, S. W., and C. H. Simonds (1980), The role of volatiles and lithology in the impact cratering process, *Rev. Geophys.*, *18*, 143–181.

Kormer, S. B. (1968), Optical study of the characteristics of shock-compressed condensed dielectrics, *Soviet Physics Usp. Engl. Transl.*, *11*(2), 229–254.

Luo, S.-N., J. A. Akins, T. J. Ahrens, and P. D. Asimow (2004), Shock-compressed $MgSiO_3$ glass, enstatite, olivine, and quartz: Optical emission, temperatures, and melting, *J. Geophys. Res.*, *109*, B05205, doi:10.1029/2003JB002860.

Lyzenga, G. A., T. J. Ahrens, W. J. Nellis, and A. C. Mitchell (1982), The temperature of shock-compressed water, *J. Chem. Phys.*, *76*, 6282–6286, doi:10.1063/1.443031.

Pierazzo, E., A. M. Vickery, and H. J. Melosh (1997), A reevaluation of impact melt production, *Icarus*, *127*, 408–423, doi:10.1006/icar.1997.5713.

Pierazzo, E., N. A. Artemieva, and B. A. Ivanov (2005), Starting conditions for hydrothermal systems underneath Martian craters: Hydrocode modeling, in *Large Meteorite Impacts III*, edited by T. Kenkmann et al., *Geol. Soc. Am. Spec. Pap.*, 384, 443–457.

Seifter, A., S. T. Stewart, M. R. Furlanetto, G. B. Kennedy, J. R. Payton, and A. W. Obst (2006), Post-shock temperature measurements of aluminum, in *Shock Compression of Condensed Matter—2005*, edited by M. D. Furnish et al., *AIP Conf. Proc.*, 845, 139–142.

Senft, L. E., and S. T. Stewart (2008), Impact crater formation in icy layered terrains on Mars, *Meteorit. Planet. Sci.*, in press.

Stewart, S. T., and T. J. Ahrens (2005), Shock properties of H_2O ice, *J. Geophys. Res.*, *110*, E03005, doi:10.1029/2004JE002305.

Stewart, S. T., J. D. O'Keefe, and T. J. Ahrens (2004), Impact processing and redistribution of near-surface water on Mars, in *Shock Compression of Condensed Matter—2003*, edited by M. D. Furnish et al., *AIP Conf. Proc.*, 706, 1484–1487.

Stewart, S. T., G. B. Kennedy, L. E. Senft, M. R. Furlanetto, A. W. Obst, J. R. Payton, and A. Seifter (2006), Post-shock temperature and free surface velocity measurements of Basalt, in *Shock Compression of Condensed Matter—2005*, edited by M. D. Furnish et al., *AIP Conf. Proc.*, 845, 1484–1487.

Trujillo, C. A., D. C. Jewitt, and J. X. Luu (2001), Properties of the trans-Neptunian belt: Statistics from the Canada-France-Hawaii Telescope survey, *Astron. J.*, *122*, 457–473, doi:10.1086/321117.

Turtle, E. P., and E. Pierazzo (2001), Thickness of a Europan ice shell from impact crater simulations, *Science*, *294*, 1326–1328, doi:10.1126/science.1062492.

Wagner, W., and A. Pruss (2002), The IAPWS formulation 1995 for the thermodynamic properties of ordinary water substance for general and scientific use, *J. Phys. Chem. Ref. Data*, *31*, 387–535, doi:10.1063/1.1461829.

Wood, C. A., J. W. Head, and M. J. Cintala (1978), Interior morphology of fresh Martian craters: The effects of target characteristics, *Proc. Lunar Planet. Sci. Conf.*, *9th*, 3691–3709.

Zahnle, K., P. Schenk, H. Levison, and L. Dones (2003), Cratering rates in the outer solar system, *Icarus*, *163*, 263–289, doi:10.1016/S0019-1035(03)00048-4.

A. W. Obst, P-23, MS H803, Los Alamos National Laboratory, Los Alamos, NM 87545, USA. (obst@lanl.gov)

A. Seifter, AOT-ABS, MS H817, Los Alamos National Laboratory, Los Alamos, NM 87545, USA. (seif@lanl.gov)

S. T. Stewart, Department of Earth and Planetary Sciences, Harvard University, 20 Oxford Street, Cambridge, MA 02138, USA. (sstewart@eps.harvard.edu)